Molecular Pairing in Twisted Bilayer Graphene Superconductivity

Yi-Jie Wang,[1,*] Geng-Dong Zhou,[1,*] Shi-Yu Peng,[2] Biao Lian,[3] and Zhi-Da Song[1,4,5,†]
[1]International Center for Quantum Materials, School of Physics, Peking University, Beijing 100871, China
[2]Applied Physics and Materials Science, California Institute of Technology, Pasadena, California 91125, USA
[3]Department of Physics, Princeton University, Princeton, New Jersey 08544, USA
[4]Hefei National Laboratory, Hefei 230088, China
[5]Collaborative Innovation Center of Quantum Matter, Beijing 100871, China

(Received 30 January 2024; revised 3 August 2024; accepted 3 September 2024; published 30 September 2024)

We propose a theory for how the weak phonon-mediated interaction ($J_A = 1$–4 meV) wins over the prohibitive Coulomb repulsion ($U = 30$–60 meV) and leads to a superconductor in magic-angle twisted bilayer graphene (MATBG). We find the pairing mechanism akin to that in the A_3C_{60} family of molecular superconductors: Each AA stacking region of MATBG resembles a C_{60} molecule, in that optical phonons can dynamically lift the degeneracy of the moiré orbitals, in analogy to the dynamical Jahn-Teller effect. Such induced J_A has the form of an intervalley anti-Hund's coupling and is less suppressed than U by the Kondo screening near a Mott insulator. Additionally, we also considered an intraorbital Hund's coupling J_H that originates from the on-site repulsion of a carbon atom. Under a reasonable approximation of the realistic model, we prove that the renormalized local interaction between quasiparticles has a pairing (negative) channel in a doped correlated insulator at $\nu = \pm(2 + \delta\nu)$, albeit the bare interaction is positive definite. The proof is nonperturbative and based on exact asymptotic behaviors of the vertex function imposed by Ward identities. Existence of an optimal U for superconductivity is predicted. In a large area of the parameter space of J_A, J_H, the ground state is found to have a nematic d-wave singlet pairing, which, however, can lead to a p-wave-like nodal structure due to the Berry's phase on Fermi surfaces (or Euler obstruction).

DOI: 10.1103/PhysRevLett.133.146001

Introduction—A striking feature of magic-angle twisted bilayer graphene (MATBG) [1] is that superconductivity (SC) emerges at small doping upon the correlated insulator (CI) [2–5]. The SC exhibits unconventional properties, such as a small coherence length [2,4], V-shaped tunneling spectrum [6], nematicity [7], and T-linear resistance [8–10]. Despite extensive research on various pairing mechanisms [11–20], understanding the coexistence of CI [21–41] and SC, and their unconventional behaviors, remains challenging. Nevertheless, experimental studies have provided some constraints on the pairing. Suppressing the CI gap by screening the Coulomb interaction may enhance SC [42–44]. Proximity-induced spin-orbit coupling enhances SC, while spontaneous ferromagnetism suppresses it, implying pairing of time-reversal partners [45,46]. These observations are consistent with a phonon-based singlet pairing mechanism, but weak coupling BCS theory cannot explain the unconventional behaviors or how the strong Coulomb repulsion [47,48] is overcome by a small attractive interaction [11–13].

Inspired by the recent experimental evidence of significant coupling between flat band electrons and A_1, B_1 phonons at $\omega_{ph} = 150$ meV [49], we examine the possibility of a pairing mechanism based on A_1, B_1 phonons. The mediated attractive interaction J_A is merely a few meV [11,13,50,51]. However, we find J_A can overcome the much stronger U if the system is close to a Mott insulator where the quenching of charge fluctuation significantly suppresses U. A prototype of this pairing mechanism is the A_3C_{60} family of molecular superconductors [52–55]. For both systems, electron orbitals are local on the scale of a superlattice—giving rise to strong correlations—but are spread on the microscopic lattice and are coupled to atomic distortions. As the A_1, B_1 phonons lead to a dynamical valley-Jahn-Teller effect [56,57], J_A plays a role similar to the anti-Hund's coupling [17] induced by the Jahn-Teller-distortion in fullerene, which is also previously suggested in Ref. [58].

Approximations and methodology—We use the topological heavy fermion (THF) model [59,60], which has recently been applied to investigate the Kondo physics in MATBG [61–71]. It consists of effective local orbitals ($f_{\alpha\eta s}$) in AA stacking regions [Fig. 1(a)], which dominate the flat bands, and itinerant Dirac c electrons, which hybridize with f orbitals to generate topology [Fig. 1(b)] [72–77]. Here $\alpha(=1,2)$, $\eta(=\pm)$, $s(=\uparrow\downarrow)$ are the orbital, valley, and spin indices, respectively.

*These authors contributed equally to this work.
†Contact author: songzd@pku.edu.cn

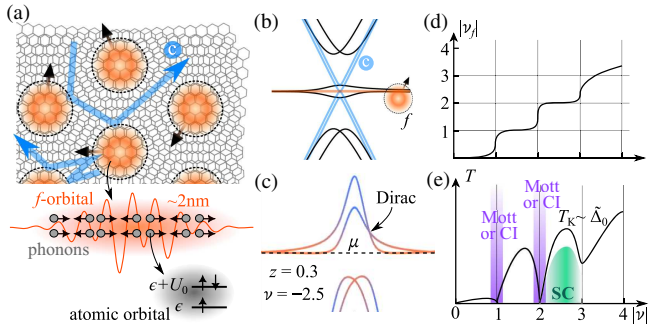

FIG. 1. Model. (a) Illustration for the effective f and c electrons. f orbitals are located at AA stacking regions and dominate the flat bands. They are coupled to microscopic phonon modes via the dynamical valley Jahn-Teller effect. (b) Energy bands (black) as a result of hybridization between f bands (orange) and itinerant Dirac c bands (blue). (c) Heavy Fermi liquid bands at $\nu=-2.5$ with the quasiparticle weight $z=0.3$. Orange and blue colors represent contributions from f and c electrons, respectively. (d) and (e) sketch the f occupation, $|\nu_f|$, and Kondo temperature, T_K, as functions of the total flat band filling $|\nu|$ in DMFT calculations in the absence of $J_{A,H}$, respectively.

Before detailed derivations, let us outline the chain of approximations and methodology employed in this Letter. After integrating out the fast A_1, B_1 phonons [51], we obtain a multiorbital Anderson lattice model where each impurity has eight flavors ($f_{\alpha\eta s}$), subject to a complex local interaction consisting of a Hubbard U term (58 meV), an anti-Hund's coupling J_A (∼1 meV), and a Hund's coupling J_H (∼1 meV) [Fig. 3(a)]. To analyze this unsolvable model, we assume the locality of correlation, treating each AA site as an Anderson impurity coupled to a bath that describes its environment. The locality of correlation is supported by the quantum-dot-like behavior [47,48] and evident local pairing gap (1–3 meV) [6,78] observed in experiments. It is also widely assumed in recent slave-particle [61,67], dynamical mean-field theory (DMFT) [62,63,65,66], and Gutzwiller [71] calculations that have reproduced key features of the experimental spectrum and compressibility [71]. Kondo temperature T_K and f occupation ν_f have been determined as functions of the total filling ν [62,63,65–67], as sketched in Fig. 1(e) and 1(d). Both ν and ν_f range from -4 to 4, with $\nu_f=\nu=0$ corresponding to the charge neutrality point. At $\nu=-2-\delta\nu$, where the highest SC T_c is observed, the ground state without $J_{A,H}$ can be a heavy Fermi liquid characterized by $T_K\sim 1$–10 K, $\nu_f\approx -2$, and a quasiparticle weight $z\sim 0.1$–0.3.

We devote this Letter to investigating the pairing instability of the Fermi liquid at $\nu=-2-\delta\nu$ in the presence of $J_{A,H}$. An immediate difficulty arises: since $U\gg J_{A,H}$, the bare interaction is positive definite and does not support any pairings [79,80] in naive mean-field theories. In fact, this difficulty will appear in any attempt

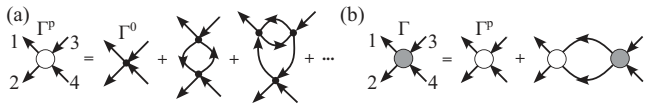

FIG. 2. Skeleton diagrams for 2PI (a) and 1PI (b) vertices. Γ^0 represents the antisymmetrized bare vertex and lines represent fully addressed Green's functions. For local 2PI and 1PI vertices, all bare vertices in the skeleton diagrams are at the same site.

to explain the SC in MATBG through a weak attractive interaction, regardless of its origin. (The Luttinger mechanism may give rise to an attractive channel but will predict a much lower SC energy scale compared to the observed local pairing gap.) A crucial step in our analysis is that, under the so-called flattened interaction limit (explained later), which is justified for the Anderson impurity in the Fermi liquid phase with $T_K\ll J_A$, we can obtain exact asymptotic behaviors of the fully renormalized local interaction. We further prove the existence of a pairing channel. This is particularly notable given that the bare interaction is positive definite.

A powerful theoretical tool that enables our analysis is the Ward identity [81–83], which relates the local one-particle irreducible (1PI) vertex, representing the renormalized local interaction, to susceptibilities (χ) of local conserved charges. The local 1PI vertex is given by skeleton diagrams (Fig. 2) of bare vertices at the same site and fully dressed local Green's functions. The behavior of χ can be known once the local ground state manifold is determined. We then derive the asymptotic behaviors of the local 1PI vertex through the Ward identity and identify a pairing channel. This approach reproduces the Bethe ansatz result for the one-orbital Anderson impurity [84], confirming its validity.

With the pairing channel identified, we next study the SC on the moiré lattice. Consider the RPA pairing susceptibility $\chi_p=\chi_{p0}/(1+\chi_{p0}\Gamma^p)$, where χ_{p0} is the noninteracting susceptibility (bubble diagram) from the heavy quasiparticle excitations on the lattice, and Γ^p is the effective local interaction. Technically, Γ^p is given by the local 2PI vertex, connected to the local 1PI vertex via Fig. 2(b), to avoid double counting in the ladder diagrams of χ_p, as is standard in many approaches [88,89]. Γ^p replaces the bare interaction in weak-coupling RPA. Instead of examining the divergence of χ_p, we perform a straightforward mean-field calculation using the effective interaction Γ^p and a renormalized quasiparticle spectrum [Fig. 1(c)]. Quantitative results, including pairing symmetry, will be discussed later.

Because of the particle-hole symmetry of the model [59,75,77,90], the physics at $\nu=2+\delta\nu$ is similar. In experiments, particle-hole asymmetry arises from various effects [91,92] including nonlocal interlayer tunneling [93].

Effective model—We write the free action for an Anderson impurity as

$$S_0 = -\sum_{\omega}\sum_{\alpha\eta s} f^{\dagger}_{\alpha\eta s}(\omega)[-i\omega + \epsilon_f - i\Delta(\omega)]f_{\alpha\eta s}(\omega). \quad (1)$$

Here ω is the fermion Matsubara frequency, ϵ_f is the on-site energy, and $\Delta(\omega)$ is the hybridization function. In a Fermi liquid phase, $\Delta(\omega)$ can be well approximated by $\Delta_0 \mathrm{sgn}(\omega)$ for low energy physics. Δ_0 should be understood as a phenomenological bare parameter that reproduces the correct T_K [94]. Our analysis in this Letter does not directly depend on Δ_0, but only on T_K. The eight flavors have identical on-site terms because they are related by time-reversal ($\eta \to \bar{\eta}$), spin ($s \to \bar{s}$), and a D_6 point group ($\alpha \to \bar{\alpha}$) symmetries [59,73]. Here indices with a bar represent the opposite indices of the same degree of freedom.

We consider three interaction terms: an on-site Hubbard U term (58 meV) contributed by Coulomb repulsion of 2D electron gas [59], an anti-Hund's coupling $J_A \approx \lambda_{RG} \times 1.3$ meV contributed by electron-phonon coupling to A_1, B_1 phonons, and a Hund's coupling $J_H \approx 0.33 \times 10^{-3} U_0$ contributed by Hubbard repulsion U_0 (3–9 eV) at each carbon atom [95–98]. The J_A term on THF basis was recently obtained in Refs. [50,51]. $\lambda_{RG} \approx 3.2$ is an enhancement factor due to the renormalization effect [99]. We also derive an analytical form of the J_H term [84]. We tabulate all the two-electron eigenstates and eigenenergies in Fig. 3(a), which completely define the four-fermion interaction Hamiltonian. As the name suggests, J_A lowers the energies of intervalley intraorbital s-wave singlet (A_1 representation) and intervalley interorbital d-wave singlets (E_2 representation) by $2J_A$ and J_A, respectively. Since U_0 disfavors double occupation on a carbon atom, and the $\alpha = 1, 2$ f orbitals are mainly distributed on the A and B graphene sublattices [59], respectively, J_H disfavors double occupation on each α orbital alike. Consequently, the interorbital d-wave singlets are energetically less penalized ($\frac{2}{3}J_H$) than the intraorbital s-wave singlets ($\frac{8}{3}J_H$).

Varying J_A and J_H over a realistic range, we thus find a large region where the lowest two-electron states are d-wave singlets [Fig. 3(d)]. In the absence of U, our single-site result fully aligns with the mean-field SC phase diagram of s-wave and d-wave pairings [11,13], where the full $\mathbf{k}$-dependent interaction is employed. However, presence of the dominating U blocks all pairing channels in the bare interaction. We thus aim to examine pairings in the renormalized interaction. As will be shown, the d-wave pairing matches several unconventional features of the SC.

Flattened interaction—To study the pairing instability of the Fermi liquid phase at $\nu = -2 - \delta\nu$, we argue that the complex interaction Hamiltonian defined by Fig. 3(a) can be replaced by a simpler one if T_K is finite but sufficiently low. When the level splittings in Fig. 3(a) far exceed the Kondo energy scale, i.e., $J_{A,H} \gg T_K$, only the two-electron ground states participate in Kondo screening [81]. Correspondingly, high-energy states turn to virtual

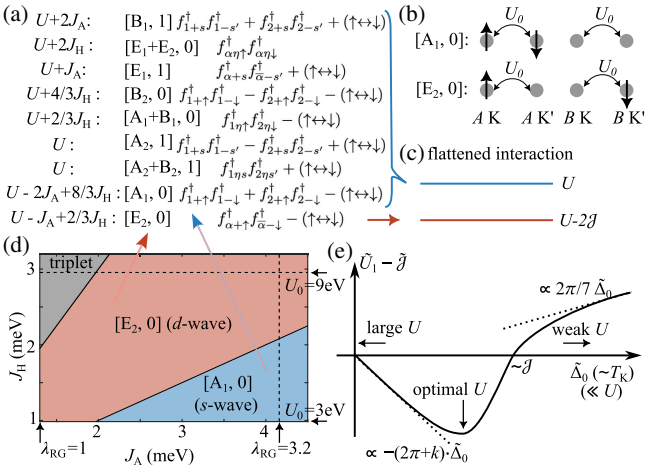

FIG. 3. Bare and renormalized interactions. (a) Two-particle eigenstates, labeled by $[\rho, j]$. ρ denotes the D_6 representation, and j denotes the total spin j. Pairing channels of the bare interaction coincide. (b) Occupations of graphene sublattices (A, B) and valleys (K, K') of the lowest E_2 and A_1 states. (c) The flattened interaction. (d) Two-electron ground states in the parameter space of J_A and J_H. As pairing channels of the bare interaction, the energies are repulsive due to U, hence they cannot form Cooper pairs. (e) The renormalized interaction $\tilde{U}_1 - \tilde{\mathcal{J}}$ for d-wave pairings as a function of the Kondo energy scale $\tilde{\Delta}_0 \sim T_K$, which is assumed to be much smaller than the bare repulsion U. With other parameters fixed, U exponentially suppresses $\tilde{\Delta}_0$, hence a smaller $\tilde{\Delta}_0$ also implies a larger U.

processes, whose splittings do not qualitatively change low energy physics. Motivated by this observation, we introduce a flattened interaction [Fig. 3(c)], where all pairing channels are set to energy U, except for the d-wave ground state that has the energy $U - 2\mathcal{J}$, with $\mathcal{J} \sim J_A \ll U$. The flattened interaction enjoys a $\mathrm{U}(1)^{\times 4} \times \mathrm{SU}(2)^{\times 2}$ symmetry generated by charge $\sigma^0\tau^0\varsigma^0$, valley τ^z, orbital σ^z, angular momentum $\sigma^z\tau^z$, and two independent spin $[(\sigma^0\tau^0 \pm \sigma^z\tau^z)/2]\varsigma^{x,y,z}$ rotations [84]. Here $\sigma^{x,y,z}$, $\tau^{x,y,z}$, and $\varsigma^{x,y,z}$ are Pauli matrices for the orbital, valley, and spin degrees of freedom, respectively. The higher symmetry gives rise to Ward identities that help determine the renormalized interaction. Notably, the flattened interaction is still positive definite and does not support pairings in naive mean-field theories.

Reference [84] provides a more quantitative justification for the flattened interaction by a phenomenological susceptibility analysis. It shows that, if the original interaction is adopted, the breaking of $\mathrm{U}(1)^{\times 4} \times \mathrm{SU}(2)^{\times 2}$ symmetry in the renormalized theory is finite but weak. The flattened interaction also applies to the $T_K \gg J_{A,H}$ limit where any multiplet splitting becomes irrelevant at the Kondo energy scale.

Constrained by the $\mathrm{U}(1)^{\times 4} \times \mathrm{SU}(2)^{\times 2}$ symmetry, a general parametrization of S_I reads

$$S_I = \frac{1}{2}\int d\tau \sum_{\alpha\eta}\Big(\Big(U_1+\frac{\mathcal{J}}{2}\Big)N_{\alpha\eta}N_{\bar{\alpha}\bar{\eta}} + U_2 N_{\alpha\eta}N_{\alpha\bar{\eta}} + U_3 N_{\alpha\eta}N_{\bar{\alpha}\eta} + U_4 N_{\bar{\alpha}\eta}^2 + 2\mathcal{J}\cdot\mathbf{S}_{\alpha\eta}\cdot\mathbf{S}_{\bar{\alpha}\bar{\eta}}\Big), \quad (2)$$

where τ is the imaginary time, $N_{\alpha\eta}$ and $\mathbf{S}_{\alpha\eta}$ are, respectively, the charge and spin operators in the valley η and orbital α. The bare flattened interaction is given by $U_1 = U - \mathcal{J}$, $U_{2,3,4} = U$, but under renormalization, the values of $U_{1,2,3,4}$ and $\mathcal{J}$ flow. The intervalley d-wave singlet (triplet) has the energy $U_1 - (+)\mathcal{J}$.

Quasiparticles in heavy Fermi liquid—In the Fermi liquid phase, the local Green's function has a quasiparticle part $z/[i\omega - \tilde{\epsilon}_f + i\tilde{\Delta}_0 \mathrm{sgn}(\omega)]$ and a featureless incoherent part. Here $z = [1 - \partial_{i\omega}\Sigma(\omega)]^{-1}|_{\omega=0}$ is the quasiparticle weight with $\Sigma(\omega)$ denoting the self-energy, $\tilde{\epsilon}_f = z[\epsilon_f + \Sigma(0)]$ is the renormalized on-site energy, and $\tilde{\Delta}_0 = z\Delta_0 \sim T_K$ is the renormalized hybridization. A typical T_K is given by $D(32\Delta_0/U)^{\frac{1}{8}}\exp[-(U/32\Delta_0)]$ if $J_{A,H} = 0$ [102], where D is the bandwidth, and T_K will be further suppressed by finite $J_{A,H}$. In this Letter, we regard $T_K \sim 1$–10 K, $\nu_f \approx -2$, and $z \sim 0.1$–0.3 [62,66] as given quantities. The ratio $\tilde{\epsilon}_f/\tilde{\Delta}_0 = \cot\delta_f$ is fixed by the occupation of f electrons via the Friedel sum rule [103], with $\delta_f = \pi(\nu_f + 4)/8 \approx (\pi/4)$.

It is convenient to define the quasiparticle operator $\tilde{f} = z^{-\frac{1}{2}}f$ [104,105], the interactions among which are given by $\tilde{\Gamma} = z^2\Gamma$, with Γ being the local 1PI vertex [Fig. 2(b)]. Because of the $\mathrm{U}(1)^{\times 4} \times \mathrm{SU}(2)^{\times 2}$ symmetry, $\tilde{\Gamma}$ is parametrized in the same form as Eq. (2), and we denote the corresponding parameters (renormalized interactions) as $\tilde{U}_{1,2,3,4}$ and $\tilde{\mathcal{J}}$.

Renormalized interaction in the $\tilde{\Delta}_0 \ll \mathcal{J} \ll U$ limit—In this limit the Kondo temperature $T_K \sim \tilde{\Delta}_0$ defines the *single* energy scale of the local Fermi liquid [81–83]. Thus, the renormalized interactions $\tilde{U}_{1,2,3,4}$, $\tilde{\mathcal{J}}$ can be expressed in terms of $\tilde{\Delta}_0$.

To derive $\tilde{U}_{1,2,3,4}$, $\tilde{\mathcal{J}}$, we make use of the Ward identities [106–108] given by the $\mathrm{U}(1)^{\times 4} \times \mathrm{SU}(2)^{\times 2}$ symmetry. They bridge the static susceptibilities χ^O of conserved charges O to the renormalized interaction $\tilde{\Gamma}$ [84]

$$\chi^O = \frac{\sin^2\delta_f}{\pi\tilde{\Delta}_0}\left[\sum_I O_I^2 - \frac{\sin^2\delta_f}{\pi\tilde{\Delta}_0}\sum_{I,I'}\tilde{\Gamma}_{I,I';I',I}O_I O_{I'}\right], \quad (3)$$

where $O = \sum_I O_I f_I^\dagger f_I$ is chosen diagonal. Setting O_I to be the electric charge $\sigma^0\tau^0\varsigma^0$ ($l = c$), spin ς^z (s), valley τ^z (v), and orbital σ^z (o) operators and exploiting $\delta_f = \pi/4$, we obtain $\chi^l = (4/\pi\tilde{\Delta}_0)[1 - (1/2\pi\tilde{\Delta}_0)\tilde{A}^l]$, with $\tilde{A}^c = 2\tilde{U}_1 + 2\tilde{U}_2 + 2\tilde{U}_3 + \tilde{U}_4 + \tilde{\mathcal{J}}$, $\tilde{A}^s = -\tilde{U}_4 + \tilde{\mathcal{J}}$, $\tilde{A}^v = -2\tilde{U}_1 - 2\tilde{U}_2 + 2\tilde{U}_3 + \tilde{U}_4 - \tilde{\mathcal{J}}$, $\tilde{A}^o = -2\tilde{U}_1 + 2\tilde{U}_2 - 2\tilde{U}_3 + \tilde{U}_4 - \tilde{\mathcal{J}}$, respectively. For the d-wave ground states [Fig. 3(a)], since the electric charge, spin, valley, and orbital degrees of freedom are frozen, i.e., they are constants in the twofold ground state manifold, the corresponding susceptibilities are not contributed by the low-energy quasiparticles [83,104,109]. Therefore, $\chi^{c,s,v,o}$ will not diverge as the quasiparticle density of states ($\sim\tilde{\Delta}_0^{-1}$) in the $\tilde{\Delta}_0 \to 0$ limit, which implies constraints $\tilde{A}^{c,s,v,o} = 2\pi\tilde{\Delta}_0$. Consequently, only one unknown parameter is left, which we choose as $\tilde{\mathcal{J}}$, and others are solved as

$$\tilde{U}_1 = -2\pi\tilde{\Delta}_0, \quad \tilde{U}_{2,3} = 2\pi\tilde{\Delta}_0 - \frac{\tilde{\mathcal{J}}}{2}, \quad \tilde{U}_4 = -2\pi\tilde{\Delta}_0 + \tilde{\mathcal{J}}. \quad (4)$$

$\tilde{U}_1$ has been determined to be negative, hence at least one of the renormalized pairing channels with energies, $\tilde{U}_1 \mp \tilde{\mathcal{J}}$ [given after Eq. (2)], must be negative. Therefore, we have proven that the renormalized interaction must possess an attractive channel at $\nu_f \approx -2$ in the $\tilde{\Delta}_0 \ll \mathcal{J}$ limit. Susceptibilities of other quantities suggest $\tilde{\mathcal{J}} = k\tilde{\Delta}_0$ with k being a constant that ranges from 4.6 to 10.3 [84]. In this region, the intervalley d-wave singlet pairing is attractive and more favored than other channels.

Renormalized interaction in the $\mathcal{J} \ll \tilde{\Delta}_0 \ll U$ limit—In this limit, $\mathcal{J}$ plays a minor role in the local Fermi liquid, and all two-electron states equally participate in the Kondo screening [81]. With an approximate U(8) symmetry, $\tilde{U}_{1,2,3,4}$ remain equal under the renormalization, whereas $\tilde{\mathcal{J}}$ remains negligible. The U(8) Ward identity leads to $\tilde{U}_{1,2,3,4} = (2\pi/7)\tilde{\Delta}_0$ [109].

The universality is lost in the intermediate regime ($\tilde{\Delta}_0 \sim \mathcal{J}$) where various two-electron states participate in the Kondo screening with unequal weights. However, the behavior of d-wave pairing strength $\tilde{U}_1 - \tilde{\mathcal{J}}$ can be inferred by an interpolating sketch between the two limits [Fig. 3(e)]. With a decreasing $\tilde{\Delta}_0$, $\tilde{U}_1 - \tilde{\mathcal{J}}$ should turn negative when $\tilde{\Delta}_0$ reaches the order of $\mathcal{J}$; when $\tilde{\Delta}_0$ is further lowered, $\tilde{U}_1 - \tilde{\mathcal{J}}$ must evolve nonmonotonically to achieve the $\tilde{\Delta}_0 \ll \mathcal{J}$ limit where $\tilde{U}_1 - \tilde{\mathcal{J}}$ vanishes linearly in $\tilde{\Delta}_0$. This suggests the existence of an optimal $\tilde{\Delta}_0$ for pairing. With the filling factor ν_f and the other bare parameters fixed, an increasing U typically suppresses the f-charge fluctuation and hence reduces $\tilde{\Delta}_0$ [102]. Therefore, Fig. 3(e) also suggests the existence of an optimal U for pairing, as observed in A_3C_{60} [52].

Quasiparticle mean-field theory—We now investigate SC on the moiré lattice (THF model) using a mean-field theory with the effective interaction $z^2\Gamma^{\mathrm{p}}$ (local 2PI vertex) and the renormalized quasiparticle spectrum [Fig. 1(c)]. Through the ladder summation [Fig. 2(b)], we find that $z^2\Gamma^{\mathrm{p}}$ has the same pairing channel as the local 1PI $z^2\Gamma$ but with a weaker potential $U_1^{\mathrm{p}} - \mathcal{J}^{\mathrm{p}} = -((2\pi + k)/\{1 + [(2\pi + k)/4]\})\tilde{\Delta}_0$ in the $\tilde{\Delta}_0 \ll \mathcal{J}$ limit [84].

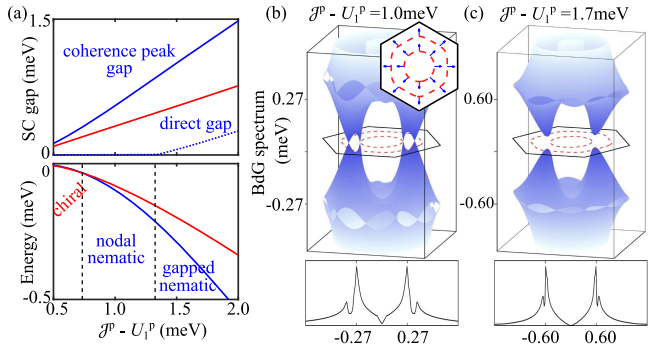

FIG. 4. Mean-field calculations of SC at $\nu = -2.5$ and $z = 0.3$. (a) Phase diagram of intervalley interorbital d-wave singlet SC. The range of $\mathcal{J}^p$–U_1^p corresponds to T_K ranging from 1.7 K to 7.1 K if $k = 8$. (b) Bogoliubov de Gennes (BdG) bands of the nematic d-wave SC with a p-wave-like nodal structure. The inset shows the $C_{2z}T$ sewing matrix phase $\phi_{\mathbf{k}}$ on the Fermi surface. (c) BdG bands of the gapped nematic d-wave SC, where the gap function is still highly anisotropic. The lower panels in (b) and (c) are the corresponding densities of states calculated using a Lorentz spread 0.004 meV.

We carry out the calculation at $\nu = -2.5$ using $z = 0.3$ and $\mathcal{J}^p - U_1^p$ in the range from 0.5 to 2 meV (Fig. 4). Including the (much weaker) nonlocal interactions does not affect the results [84]. Since the d-wave pairings form the two-dimensional representation E_2, we find two possible phases. One is a gapped chiral d-wave pairing $\tilde{f}^\dagger_{\mathbf{k}\alpha+\uparrow}\tilde{f}^\dagger_{-\mathbf{k}\bar{\alpha}-\downarrow} - (\uparrow \leftrightarrow \downarrow)$ (for either $\alpha = 1$ or 2). The other is a nematic d-wave pairing [11,13,17,18] $e^{-i\varphi}\tilde{f}^\dagger_{\mathbf{k}1+\uparrow}\tilde{f}^\dagger_{-\mathbf{k}2-\downarrow} + e^{i\varphi}\tilde{f}^\dagger_{\mathbf{k}2+\uparrow}\tilde{f}^\dagger_{-\mathbf{k}1-\downarrow} - (\uparrow \leftrightarrow \downarrow)$ that breaks the C_{3z} symmetry. Here φ sets the orientation of the nematic order. When $\mathcal{J}^p - U_1^p < 0.7$ meV, the chiral state has a slightly lower energy than the nematic state. When $\mathcal{J}^p - U_1^p > 0.7$ meV, the nematic state has a significantly lower energy than the chiral state.

p-wave-like nodal SC—An intermediate pairing strength leads to a p-wave-like nodal structure, as shown in Fig. 4(b). We now prove that the 2 (mod 4) nodes on each Fermi surface (FS) are guaranteed by the π Berry's phase protected by $C_{2z}T$ symmetry. Suppose $\psi_{\mathbf{k}+s}$ is the annihilation operator for Bloch states on a given FS in the $\eta = +$ valley, and $(C_{2z}T)\psi^\dagger_{\mathbf{k}+s}(C_{2z}T)^{-1} = \psi^\dagger_{\mathbf{k}+s}e^{i\phi_{\mathbf{k}}}$. Because of $(C_{2z}T)\tilde{f}^\dagger_{\mathbf{k}\alpha\eta s}(C_{2z}T)^{-1} = \tilde{f}^\dagger_{\mathbf{k}\bar{\alpha}\eta s}$ [59,84], there must be $\psi^\dagger_{\mathbf{k}+s} \sim \tilde{f}^\dagger_{\mathbf{k}1+s} + e^{-i\phi_{\mathbf{k}}}\tilde{f}^\dagger_{\mathbf{k}2+s}$. Bloch states in the $\eta = -$ valley can be obtained by applying the time reversal: $\psi^\dagger_{-\mathbf{k}-s} \sim \tilde{f}^\dagger_{-\mathbf{k}1-s} + e^{i\phi_{\mathbf{k}}}\tilde{f}^\dagger_{-\mathbf{k}2-s}$. Projecting the nematic d-wave pairing onto the FS, we obtain $\cos(\phi_{\mathbf{k}} + \varphi) \cdot \psi^\dagger_{\mathbf{k}+\uparrow}\psi^\dagger_{-\mathbf{k}-\downarrow} - (\uparrow \leftrightarrow \downarrow)$. As the FS encloses an odd number of Dirac points [Fig. 1(c)], $\phi_{\mathbf{k}}$ must wind an odd $(2n+1)$ multiple of 2π along the FS [Fig. 4(b)] [76], leaving $4n+2$ nodes at $\phi_{\mathbf{k}} + \varphi = \pm(\pi/2)$. As detailed in Ref. [84], an alternative understanding of the pairing nodes is the Euler obstruction [14].

As the pairing becomes stronger, nodes on the two FSs will merge, leading to a gapped phase [Fig. 4(c)]. The spectrum of the gapped nematic SC remains highly anisotropic if the direct gap is significantly smaller than the pairing. Therefore, both the nodal and the gapped nematic d-wave SC can have a V-shaped density of states at an energy scale larger than the direct gap (0 in the nodal case). This is consistent with the V-shaped spectrum [6] and nematicity [7] seen in experiments.

Discussion—Our theory provides insights into the strong coupling features of SC in MATBG. The pairing potential $\mathcal{J}^p - U_1^p$ is a few times larger than T_K, and the Fermi energy $E_F \sim T_K$ [Fig. 1(c)]. Therefore, $\mathcal{J}^p - U_1^p \gtrsim E_F$, suggesting the SC is closer to a BEC state than a BCS state [2,4]. Pairings are localized around "moiré molecules" in AA-stacking regions, leading to a smaller phase stiffness —only contributed by hybridization with Dirac electrons in AB regions—compared to BCS pairings of delocalized states [110]. This may explain the large ratio between the pairing gap and T_c [6].

In the intermediate regime where $T_K \sim J_A$, multiplet splittings breaking the $U(1)^{\times 4} \times SU(2)^{\times 2}$ symmetry should be considered. The remaining Ward identities cannot fully constrain the renormalized interaction. However, the continuity [Fig. 3(e)] suggests pairing is still possible. We leave this for future studies.

Acknowledgments—We are grateful to Xi Dai for helpful discussions about the A_3C_{60} family of superconductors. We thank B. Andrei Bernevig and Jiabin Yu for helpful discussions about nodal pairings. We also thank Chang-Ming Yue, Xiao-Bo Lu, and Seung-Sup Lee for useful discussions. Z.-D. S., Y.-J. W., and G.-D. Z. were supported by National Natural Science Foundation of China (General Program No. 12274005), National Key Research and Development Program of China (No. 2021YFA1401900), and Innovation Program for Quantum Science and Technology (No. 2021ZD0302403). B. L. is supported by the National Science Foundation under Award No. DMR-2141966, and the National Science Foundation through Princeton University's Materials Research Science and Engineering Center DMR-2011750.

[1] Rafi Bistritzer and Allan H. MacDonald, Moiré bands in twisted double-layer graphene, Proc. Natl. Acad. Sci. U.S.A. **108**, 12233 (2011).

[2] Yuan Cao, Valla Fatemi, Shiang Fang, Kenji Watanabe, Takashi Taniguchi, Efthimios Kaxiras, and Pablo Jarillo-Herrero, Unconventional superconductivity in magic-angle graphene superlattices, Nature (London) **556**, 43 (2018).

[3] Yuan Cao, Valla Fatemi, Ahmet Demir, Shiang Fang, Spencer L. Tomarken, Jason Y. Luo, Javier D. Sanchez-Yamagishi, Kenji Watanabe, Takashi Taniguchi, Efthimios Kaxiras, Ray C. Ashoori, and Pablo Jarillo-Herrero, Correlated insulator behaviour at half-filling in

magic-angle graphene superlattices, Nature (London) **556**, 80 (2018).

[4] Xiaobo Lu, Petr Stepanov, Wei Yang, Ming Xie, Mohammed Ali Aamir, Ipsita Das, Carles Urgell, Kenji Watanabe, Takashi Taniguchi, Guangyu Zhang, Adrian Bachtold, Allan H. MacDonald, and Dmitri K. Efetov, Superconductors, orbital magnets and correlated states in magic-angle bilayer graphene, Nature (London) **574**, 653 (2019).

[5] Matthew Yankowitz, Shaowen Chen, Hryhoriy Polshyn, Yuxuan Zhang, K. Watanabe, T. Taniguchi, David Graf, Andrea F. Young, and Cory R. Dean, Tuning superconductivity in twisted bilayer graphene, Science **363**, 1059 (2019).

[6] Myungchul Oh, Kevin P. Nuckolls, Dillon Wong, Ryan L. Lee, Xiaomeng Liu, Kenji Watanabe, Takashi Taniguchi, and Ali Yazdani, Evidence for unconventional superconductivity in twisted bilayer graphene, Nature (London) **600**, 240 (2021).

[7] Yuan Cao, Daniel Rodan-Legrain, Jeong Min Park, Noah F. Q. Yuan, Kenji Watanabe, Takashi Taniguchi, Rafael M. Fernandes, Liang Fu, and Pablo Jarillo-Herrero, Nematicity and competing orders in superconducting magic-angle graphene, Science **372**, 264 (2021).

[8] Y. Cao, D. Chowdhury, D. Rodan-Legrain, O. Rubies-Bigorda, K. Watanabe, T. Taniguchi, T. Senthil, and P. Jarillo-Herrero, Strange metal in magic-angle graphene with near Planckian dissipation, Phys. Rev. Lett. **124**, 076801 (2020).

[9] Hryhoriy Polshyn, Matthew Yankowitz, Shaowen Chen, Yuxuan Zhang, K. Watanabe, T. Taniguchi, Cory R. Dean, and Andrea F. Young, Large linear-in-temperature resistivity in twisted bilayer graphene, Nat. Phys. **15**, 1011 (2019).

[10] Alexandre Jaoui, Ipsita Das, Giorgio Di Battista, Jaime Díez-Mérida, Xiaobo Lu, Kenji Watanabe, Takashi Taniguchi, Hiroaki Ishizuka, Leonid Levitov, and Dmitri K. Efetov, Quantum critical behaviour in magic-angle twisted bilayer graphene, Nat. Phys. **18**, 633 (2022).

[11] Fengcheng Wu, A. H. MacDonald, and Ivar Martin, Theory of phonon-mediated superconductivity in twisted bilayer graphene, Phys. Rev. Lett. **121**, 257001 (2018).

[12] B. Lian, Z. Wang, and B. A. Bernevig, Twisted bilayer graphene: A phonon-driven superconductor, Phys. Rev. Lett. **122**, 257002 (2019).

[13] C. X. Liu, Y. Chen, A. Yazdani, and B. A. Bernevig, Electron–K-phonon interaction in twisted bilayer graphene, Phys. Rev. B **110**, 045133 (2024).

[14] Jiabin Yu, Ming Xie, Fengcheng Wu, and Sankar Das Sarma, Euler obstructed Cooper pairing in twisted bilayer graphene: Nematic nodal superconductivity and bounded superfluid weight, Phys. Rev. B **105**, 104515 (2022).

[15] Yi-Zhuang You and Ashvin Vishwanath, Superconductivity from valley fluctuations and approximate SO(4) symmetry in a weak coupling theory of twisted bilayer graphene, npj Quantum Mater. **4**, 1 (2019).

[16] Eslam Khalaf, Shubhayu Chatterjee, Nick Bultinck, Michael P. Zaletel, and Ashvin Vishwanath, Charged skyrmions and topological origin of superconductivity in magic-angle graphene, Sci. Adv. **7**, eabf5299 (2021).

[17] Andrea Blason and Michele Fabrizio, Local Kekulé distortion turns twisted bilayer graphene into topological Mott insulators and superconductors, Phys. Rev. B **106**, 235112 (2022).

[18] Tomas Löthman, Johann Schmidt, Fariborz Parhizgar, and Annica M. Black-Schaffer, Nematic superconductivity in magic-angle twisted bilayer graphene from atomistic modeling, Commun. Phys. **5**, 1 (2022).

[19] Maine Christos, Subir Sachdev, and Mathias S. Scheurer, Nodal band-off-diagonal superconductivity in twisted graphene superlattices, Nat. Commun. **14**, 7134 (2023).

[20] SK Firoz Islam, A. Y. Zyuzin, and A. A. Zyuzin, Unconventional superconductivity with preformed pairs in twisted bilayer graphene, Phys. Rev. B **107**, L060503 (2023).

[21] Hoi Chun Po, Liujun Zou, Ashvin Vishwanath, and T. Senthil, Origin of Mott insulating behavior and superconductivity in twisted bilayer graphene, Phys. Rev. X **8**, 031089 (2018).

[22] Nick Bultinck, Eslam Khalaf, Shang Liu, Shubhayu Chatterjee, Ashvin Vishwanath, and Michael P. Zaletel, Ground state and hidden symmetry of magic-angle graphene at even integer filling, Phys. Rev. X **10**, 031034 (2020).

[23] Jian Kang and Oskar Vafek, Strong coupling phases of partially filled twisted bilayer graphene narrow bands, Phys. Rev. Lett. **122**, 246401 (2019).

[24] B. Lian, Z. D. Song, N. Regnault, D. K. Efetov, A. Yazdani, and B. A. Bernevig, Twisted bilayer graphene. IV. Exact insulator ground states and phase diagram, Phys. Rev. B **103**, 205414 (2021).

[25] F. Xie, A. Cowsik, Z. D. Song, B. Lian, B. A. Bernevig, and N. Regnault, Twisted bilayer graphene. VI. An exact diagonalization study at nonzero integer filling, Phys. Rev. B **103**, 205416 (2021).

[26] Jianpeng Liu and Xi Dai, Theories for the correlated insulating states and quantum anomalous Hall effect phenomena in twisted bilayer graphene, Phys. Rev. B **103**, 035427 (2021).

[27] Dante M. Kennes, Johannes Lischner, and Christoph Karrasch, Strong correlations and $d + id$ superconductivity in twisted bilayer graphene, Phys. Rev. B **98**, 241407 (R) (2018).

[28] Mikito Koshino, Noah F. Q. Yuan, Takashi Koretsune, Masayuki Ochi, Kazuhiko Kuroki, and Liang Fu, Maximally localized Wannier orbitals and the extended hubbard model for twisted bilayer graphene, Phys. Rev. X **8**, 031087 (2018).

[29] Xiao Yan Xu, K. T. Law, and Patrick A. Lee, Kekulé valence bond order in an extended Hubbard model on the honeycomb lattice with possible applications to twisted bilayer graphene, Phys. Rev. B **98**, 121406(R) (2018).

[30] Jörn W. F. Venderbos and Rafael M. Fernandes, Correlations and electronic order in a two-orbital honeycomb lattice model for twisted bilayer graphene, Phys. Rev. B **98**, 245103 (2018).

[31] Masayuki Ochi, Mikito Koshino, and Kazuhiko Kuroki, Possible correlated insulating states in magic-angle twisted

bilayer graphene under strongly competing interactions, Phys. Rev. B **98**, 081102(R) (2018).
[32] Kangjun Seo, Valeri N. Kotov, and Bruno Uchoa, Ferromagnetic Mott state in twisted graphene bilayers at the magic angle, Phys. Rev. Lett. **122**, 246402 (2019).
[33] Laura Classen, Carsten Honerkamp, and Michael M. Scherer, Competing phases of interacting electrons on triangular lattices in moiré heterostructures, Phys. Rev. B **99**, 195120 (2019).
[34] Jian Kang and Oskar Vafek, Non-Abelian Dirac node braiding and near-degeneracy of correlated phases at odd integer filling in magic-angle twisted bilayer graphene, Phys. Rev. B **102**, 035161 (2020).
[35] Ming Xie and A. H. MacDonald, Nature of the correlated insulator states in twisted bilayer graphene, Phys. Rev. Lett. **124**, 097601 (2020).
[36] Tommaso Cea and Francisco Guinea, Band structure and insulating states driven by Coulomb interaction in twisted bilayer graphene, Phys. Rev. B **102**, 045107 (2020).
[37] Yi Zhang, Kun Jiang, Ziqiang Wang, and Fuchun Zhang, Correlated insulating phases of twisted bilayer graphene at commensurate filling fractions: A Hartree-Fock study, Phys. Rev. B **102**, 035136 (2020).
[38] Tomohiro Soejima, Daniel E. Parker, Nick Bultinck, Johannes Hauschild, and Michael P. Zaletel, Efficient simulation of moiré materials using the density matrix renormalization group, Phys. Rev. B **102**, 205111 (2020).
[39] Shang Liu, Eslam Khalaf, Jong Yeon Lee, and Ashvin Vishwanath, Nematic topological semimetal and insulator in magic-angle bilayer graphene at charge neutrality, Phys. Rev. Res. **3**, 013033 (2021).
[40] Y. D. Liao, J. Kang, C. N. Breiø, X. Y. Xu, H. Q. Wu, B. M. Andersen, R. M. Fernandes, and Z. Y. Meng, Correlation-induced insulating topological phases at charge neutrality in twisted bilayer graphene, Phys. Rev. X **11**, 011014 (2021).
[41] Kasra Hejazi, Xiao Chen, and Leon Balents, Hybrid Wannier Chern bands in magic angle twisted bilayer graphene and the quantized anomalous Hall effect, Phys. Rev. Res. **3**, 013242 (2021).
[42] Petr Stepanov, Ipsita Das, Xiaobo Lu, Ali Fahimniya, Kenji Watanabe, Takashi Taniguchi, Frank H. L. Koppens, Johannes Lischner, Leonid Levitov, and Dmitri K. Efetov, Untying the insulating and superconducting orders in magic-angle graphene, Nature (London) **583**, 375 (2020).
[43] Yu Saito, Jingyuan Ge, Kenji Watanabe, Takashi Taniguchi, and Andrea F. Young, Independent superconductors and correlated insulators in twisted bilayer graphene, Nat. Phys. **16**, 926 (2020).
[44] Xiaoxue Liu, Zhi Wang, K. Watanabe, T. Taniguchi, Oskar Vafek, and J. I. A. Li, Tuning electron correlation in magic-angle twisted bilayer graphene using Coulomb screening, Science **371**, 1261 (2021).
[45] Harpreet Singh Arora, Robert Polski, Yiran Zhang, Alex Thomson, Youngjoon Choi, Hyunjin Kim, Zhong Lin, Ilham Zaky Wilson, Xiaodong Xu, Jiun-Haw Chu, Kenji Watanabe, Takashi Taniguchi, Jason Alicea, and Stevan Nadj-Perge, Superconductivity in metallic twisted bilayer graphene stabilized by WSe2, Nature (London) **583**, 379 (2020).
[46] Jiang-Xiazi Lin, Ya-Hui Zhang, Erin Morissette, Zhi Wang, Song Liu, Daniel Rhodes, K. Watanabe, T. Taniguchi, James Hone, and J. I. A. Li, Spin-orbit–driven ferromagnetism at half moiré filling in magic-angle twisted bilayer graphene, Science **375**, 437 (2022).
[47] Dillon Wong, Kevin P. Nuckolls, Myungchul Oh, Biao Lian, Yonglong Xie, Sangjun Jeon, Kenji Watanabe, Takashi Taniguchi, B. Andrei Bernevig, and Ali Yazdani, Cascade of electronic transitions in magic-angle twisted bilayer graphene, Nature (London) **582**, 198 (2020).
[48] Youngjoon Choi, Hyunjin Kim, Cyprian Lewandowski, Yang Peng, Alex Thomson, Robert Polski, Yiran Zhang, Kenji Watanabe, Takashi Taniguchi, Jason Alicea, and Stevan Nadj-Perge, Interaction-driven band flattening and correlated phases in twisted bilayer graphene, Nat. Phys. **17**, 1375 (2021).
[49] Cheng Chen, Kevin P Nuckolls, Shuhan Ding, Wangqian Miao, Dillon Wong, Myungchul Oh, Ryan L Lee, Shanmei He, Cheng Peng, Ding Pei *et al.*, Strong inter-valley electron-phonon coupling in magic-angle twisted bilayer graphene, arXiv:2303.14903.
[50] Hao Shi, Wangqian Miao, and Xi Dai, Moiré optical phonons dancing with heavy electrons in magic-angle twisted bilayer graphene, arXiv:2402.11824.
[51] Yi-Jie Wang, Geng-Dong Zhou, Biao Lian, and Zhi-Da Song, Electron phonon coupling in the topological heavy fermion model of twisted bilayer graphene, arXiv:2407.11116.
[52] Massimo Capone, Michele Fabrizio, Claudio Castellani, and Erio Tosatti, Colloquium: Modeling the unconventional superconducting properties of expanded A_3C_{60} fullerides, Rev. Mod. Phys. **81**, 943 (2009).
[53] M. Capone, M. Fabrizio, C. Castellani, and E. Tosatti, Strongly correlated superconductivity, Science **296**, 2364 (2002).
[54] Sudip Chakravarty, Martin P. Gelfand, and Steven Kivelson, Electronic correlation effects and superconductivity in doped fullerenes, Science **254**, 970 (1991).
[55] Assa Auerbach, Nicola Manini, and Erio Tosatti, Electron-vibron interactions in charged fullerenes. I. Berry phases, Phys. Rev. B **49**, 12998 (1994).
[56] M. Angeli, E. Tosatti, and M. Fabrizio, Valley Jahn-Teller effect in twisted bilayer graphene, Phys. Rev. X **9**, 041010 (2019).
[57] Mattia Angeli and Michele Fabrizio, Jahn–Teller coupling to moiré phonons in the continuum model formalism for small-angle twisted bilayer graphene, Eur. Phys. J. Plus **135**, 630 (2020).
[58] J. F. Dodaro, S. A. Kivelson, Y. Schattner, X. Q. Sun, and C. Wang, Phases of a phenomenological model of twisted bilayer graphene, Phys. Rev. B **98**, 075154 (2018).
[59] Z. D. Song and B. A. Bernevig, Magic-angle twisted bilayer graphene as a topological heavy fermion problem, Phys. Rev. Lett. **129**, 047601 (2022).
[60] Hao Shi and Xi Dai, Heavy-fermion representation for twisted bilayer graphene systems, Phys. Rev. B **106**, 245129 (2022).

[61] Yang-Zhi Chou and Sankar Das Sarma, Kondo lattice model in magic-angle twisted bilayer graphene, Phys. Rev. Lett. **131**, 026501 (2023).
[62] Geng-Dong Zhou, Yi-Jie Wang, Ninghua Tong, and Zhi-Da Song, Kondo phase in twisted bilayer graphene, Phys. Rev. B **109**, 045419 (2024).
[63] H. Hu, G. Rai, L. Crippa, J. Herzog-Arbeitman, D. Călugăru, T. Wehling, G. Sangiovanni, R. Valentí, A. M. Tsvelik, and B. A. Bernevig, Symmetric Kondo lattice states in doped strained twisted bilayer graphene, Phys. Rev. Lett. **131**, 166501 (2023).
[64] H. Hu, B. A. Bernevig, and A. M. Tsvelik, Kondo lattice model of magic-angle twisted-bilayer graphene: Hund's rule, local-moment fluctuations, and low-energy effective theory, Phys. Rev. Lett. **131**, 026502 (2023).
[65] Anushree Datta, M. J. Calderón, A. Camjayi, and E. Bascones, Heavy quasiparticles and cascades without symmetry breaking in twisted bilayer graphene, Nat. Commun. **14**, 5036 (2023).
[66] Gautam Rai, Lorenzo Crippa, Dumitru Călugăru, Haoyu Hu, Luca de' Medici, Antoine Georges, B. Andrei Bernevig, Roser Valentí, Giorgio Sangiovanni, and Tim Wehling, Dynamical correlations and order in magic-angle twisted bilayer graphene, Phys. Rev. X **14**, 031045.
[67] Liam L. H. Lau and Piers Coleman, Topological mixed valence model for twisted bilayer graphene, arXiv: 2303.02670.
[68] Yang-Zhi Chou and Sankar Das Sarma, Scaling theory of intrinsic Kondo and Hund's rule interactions in magic-angle twisted bilayer graphene, Phys. Rev. B **108**, 125106 (2023).
[69] Rafael Luque Merino, Dumitru Calugaru, Haoyu Hu, Jaime Diez-Merida, Andres Diez-Carlon, Takashi Taniguchi, Kenji Watanabe, Paul Seifert, B. Andrei Bernevig, and Dmitri K. Efetov, Evidence of heavy fermion physics in the thermoelectric transport of magic angle twisted bilayer graphene, arXiv:2402.11749v1.
[70] Dumitru Călugăru, Haoyu Hu, Rafael Luque Merino, Nicolas Regnault, Dmitri K. Efetov, and B. Andrei Bernevig, The thermoelectric effect and its natural heavy fermion explanation in twisted bilayer and trilayer graphene, arXiv:2402.14057.
[71] Qianying Hu, Shu Liang, Xinheng Li, Hao Shi, Xi Dai, and Yang Xu, Link between cascade transitions and correlated Chern insulators in magic-angle twisted bilayer graphene, arXiv:2406.08734.
[72] Hoi Chun Po, Liujun Zou, T. Senthil, and Ashvin Vishwanath, Faithful tight-binding models and fragile topology of magic-angle bilayer graphene, Phys. Rev. B **99**, 195455 (2019).
[73] Z. Song, Z. Wang, W. Shi, G. Li, C. Fang, and B. A. Bernevig, All magic angles in twisted bilayer graphene are topological, Phys. Rev. Lett. **123**, 036401 (2019).
[74] Grigory Tarnopolsky, Alex Jura Kruchkov, and Ashvin Vishwanath, Origin of magic angles in twisted bilayer graphene, Phys. Rev. Lett. **122**, 106405 (2019).
[75] Z. D. Song, B. Lian, N. Regnault, and B. A. Bernevig, Twisted bilayer graphene. II. Stable symmetry anomaly, Phys. Rev. B **103**, 205412 (2021).
[76] Junyeong Ahn, Sungjoon Park, and Bohm-Jung Yang, Failure of Nielsen-Ninomiya theorem and fragile topology in two-dimensional systems with space-time inversion symmetry: Application to twisted bilayer graphene at magic angle, Phys. Rev. X **9**, 021013 (2019).
[77] Jie Wang, Yunqin Zheng, Andrew J. Millis, and Jennifer Cano, Chiral approximation to twisted bilayer graphene: Exact intravalley inversion symmetry, nodal structure, and implications for higher magic angles, Phys. Rev. Res. **3**, 023155 (2021).
[78] Hyunjin Kim, Youngjoon Choi, Cyprian Lewandowski, Alex Thomson, Yiran Zhang, Robert Polski, Kenji Watanabe, Takashi Taniguchi, Jason Alicea, and Stevan Nadj-Perge, Evidence for unconventional superconductivity in twisted trilayer graphene, Nature (London) **606**, 494 (2022).
[79] B. A. Bernevig, B. Lian, A. Cowsik, F. Xie, N. Regnault, and Z. D. Song, Twisted bilayer graphene. V. Exact analytic many-body excitations in Coulomb Hamiltonians: Charge gap, Goldstone modes, and absence of Cooper pairing, Phys. Rev. B **103**, 205415 (2021).
[80] Debanjan Chowdhury, Interactions, topology and quantum criticality in moiré transition metal dichalcogenide materials, *Talk at the "Young Research Leaders in Topological Materials and Beyond' 24 " Workshop, Hong Kong* (2024).
[81] Ph Nozières and A. Blandin, Kondo effect in real metals, J. Phys. **41**, 193 (1980).
[82] P. Coleman, Heavy fermions: Electrons at the edge of magnetism, in *Handbook of Magnetism and Advanced Magnetic Materials*, edited by H. Kronmuller and S. Parkin (John Wiley and Sons, New York, 2007).
[83] A C Hewson, Fermi liquid theory and magnetic impurity systems. I. Quasi-particle Hamiltonians and mean field theory, J. Phys. Condens. Matter **5**, 6277 (1993).
[84] See Supplemental Material at http://link.aps.org/supplemental/10.1103/PhysRevLett.133.146001 for detailed description of the local interaction, the solution to the Anderson impurity problem with the flattened and the original interactions, and the quasiparticle mean-field theory of the superconductivity. The Supplementary Material also includes Refs. [85–87].
[85] Vasileios Pandis, Development and application of renormalised perturbation theory to models with strongly correlated electrons, Ph.D. thesis, Department of Mathematics, Imperial College London, 2015.
[86] Norio Kawakami and Ayao Okiji, Ground state of Anderson Hamiltonian, J. Phys. Soc. Jpn. **51**, 1145 (1982).
[87] P. B. Wiegmann and A. M. Tsvelick, Exact solution of the Anderson model: I, J. Phys. C **16**, 2281 (1983).
[88] Antoine Georges, Gabriel Kotliar, Werner Krauth, and Marcelo J. Rozenberg, Dynamical mean-field theory of strongly correlated fermion systems and the limit of infinite dimensions, Rev. Mod. Phys. **68**, 13 (1996).
[89] G. Rohringer, H. Hafermann, A. Toschi, A. A. Katanin, A. E. Antipov, M. I. Katsnelson, A. I. Lichtenstein, A. N. Rubtsov, and K. Held, Diagrammatic routes to nonlocal correlations beyond dynamical mean field theory, Rev. Mod. Phys. **90**, 025003 (2018).

[90] B. A. Bernevig, Z. D. Song, Nicolas Regnault, and Biao Lian, Twisted bilayer graphene. III. Interacting Hamiltonian and exact symmetries, Phys. Rev. B **103**, 205413 (2021).
[91] Jian Kang and Oskar Vafek, Pseudomagnetic fields, particle-hole asymmetry, and microscopic effective continuum Hamiltonians of twisted bilayer graphene, Phys. Rev. B **107**, 075408 (2023).
[92] Jonah Herzog-Arbeitman, Jiabin Yu, Dumitru Călugăru, Haoyu Hu, Nicolas Regnault, Oskar Vafek, Jian Kang, and B. Andrei Bernevig, Heavy fermions as an efficient representation of atomistic strain and relaxation in twisted bilayer graphene, arXiv:2405.13880.
[93] Y. H. Kwan, G. Wagner, T. Soejima, M. P. Zaletel, S. H. Simon, S. A. Parameswaran, and N. Bultinck, Kekulé spiral order at all nonzero integer fillings in twisted bilayer graphene, Phys. Rev. X **11**, 041063 (2021).
[94] Δ_0 could be estimated from self-consistent hybridization function in DMFT calculation.
[95] T. O. Wehling, E. Şaşıoğlu, C. Friedrich, A. I. Lichtenstein, M. I. Katsnelson, and S. Blügel, Strength of effective Coulomb interactions in graphene and graphite, Phys. Rev. Lett. **106**, 236805 (2011), U_0 is estimated as 9.3 eV.
[96] M. Schüler, M. Rösner, T. O. Wehling, A. I. Lichtenstein, and M. I. Katsnelson, Optimal Hubbard models for materials with nonlocal Coulomb interactions: Graphene, silicene, and benzene, Phys. Rev. Lett. **111**, 036601 (2013), the bare and effective U_0 are estimated as 10.2 and 4.5 eV, respectively.
[97] L. A. Gonzalez-Arraga, J. L. Lado, Francisco Guinea, and P. San-Jose, Electrically controllable magnetism in twisted bilayer graphene, Phys. Rev. Lett. **119**, 107201 (2017).
[98] Shihao Zhang, Xi Dai, and Jianpeng Liu, Spin-polarized nematic order, quantum valley Hall states, and field-tunable topological transitions in twisted multilayer graphene systems, Phys. Rev. Lett. **128**, 026403 (2022).
[99] D. M. Basko and I. L. Aleiner, Interplay of Coulomb and electron-phonon interactions in graphene, Phys. Rev. B **77**, 041409(R) (2008). The renormalization of J_A has also been considered in mean-field calculations [100] to obtain the Kekulé order seen in the CI at $\nu = -2$ [101].
[100] Yves H. Kwan, Glenn Wagner, Nick Bultinck, Steven H. Simon, Erez Berg, and S. A. Parameswaran, Electron-phonon coupling and competing Kekulé orders in twisted bilayer graphene, arXiv:2303.13602.
[101] Kevin P. Nuckolls, Ryan L. Lee, Myungchul Oh, Dillon Wong, Tomohiro Soejima, Jung Pyo Hong, Dumitru Călugăru, Jonah Herzog-Arbeitman, B. Andrei Bernevig, Kenji Watanabe, Takashi Taniguchi, Nicolas Regnault, Michael P. Zaletel, and Ali Yazdani, Quantum textures of the many-body wavefunctions in magic-angle graphene, Nature (London) **620**, 525 (2023).
[102] Piers Coleman, *Introduction to Many-Body Physics* (Cambridge University Press, Cambridge, England, 2015) see 17.40 for the expression of T_K in large N limit, where $J\rho$ there are $4\Delta/U$ here by Schrieffer-Wolff transformation.
[103] Hiroyuki Shiba, The Korringa relation for the impurity nuclear spin-lattice relaxation in dilute Kondo alloys, Prog. Theor. Phys. **54**, 967 (1975).
[104] A. C. Hewson, Renormalized perturbation expansions and Fermi liquid theory, Phys. Rev. Lett. **70**, 4007 (1993).
[105] A C Hewson, Renormalized perturbation calculations for the single-impurity Anderson model, J. Phys. Condens. Matter **13**, 10011 (2001).
[106] Kosaku Yamada, Perturbation expansion for the Anderson Hamiltonian. II, Prog. Theor. Phys. **53**, 970 (1975).
[107] Kosaku Yamada, Perturbation expansion for the Anderson Hamiltonian. IV, Prog. Theor. Phys. **54**, 316 (1975).
[108] Akio Yoshimori, Perturbation analysis on orbital-degenerate Anderson model, Prog. Theor. Phys. **55**, 67 (1976).
[109] Y. Nishikawa, D. J. G. Crow, and A. C. Hewson, Renormalized parameters and perturbation theory for an n-channel Anderson model with Hund's rule coupling: Symmetric case, Phys. Rev. B **82**, 115123 (2010).
[110] Fang Xie, Zhida Song, Biao Lian, and B. A. Bernevig, Topology-bounded superfluid weight in twisted bilayer graphene, Phys. Rev. Lett. **124**, 167002 (2020).